Electronic Supplementary Material (ESI) for Nanoscale.

Supporting Information

High-temperature superconductivity at the lanthanum cuprate/lanthanum-strontium nickelate interface

Federico Baiutti, Giuliano Gregori, Y. Eren Suyolcu, Yi Wang, Georg Cristiani, Wilfried Sigle, Peter A. van Aken, Gennady Logvenov,* and *Joachim Maier*

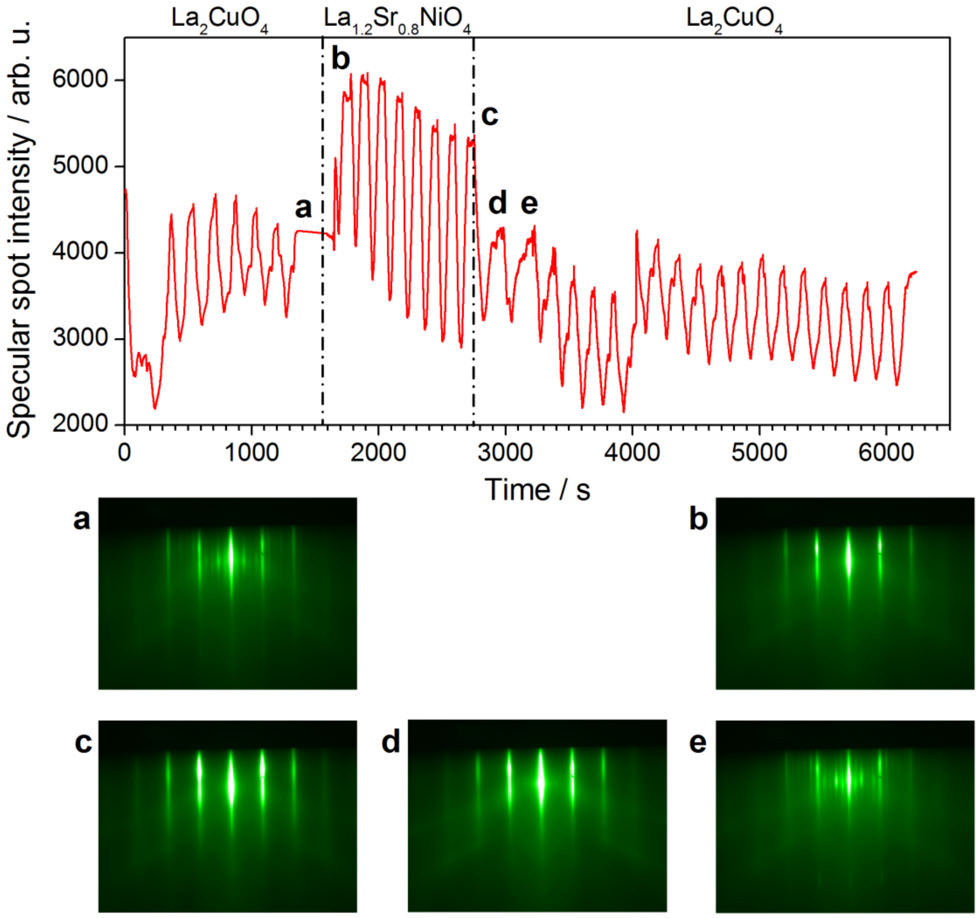

Supplementary Figure S1. Time evolution of the RHEED specular spot intensity recorded during the deposition of a trilayer structure of 4 u.c. La_2CuO_4 / 4 u.c. $La_{1.2}Sr_{0.8}NiO_4$ / 10 u.c. La_2CuO_4 on $LaSrAlO_4$ substrate. Different diffraction patterns can be recognized. In particular, the bottom La_2CuO_4 layer exhibits the typical features of the phase, including the superstructure lines between the main streaks (a). During the growth of $La_{1.2}Sr_{0.8}NiO_4$, no secondary phases outgrowths are detected (panel (b) and (c)). The top La_2CuO_4 layer grows epitaxially (d) and exhibit finite superstructure lines starting from the second monolayer (e). The absence of the superstructure in (d) is indicative of a certain crystallographic disorder at the interface. During the entire growth, pronounced RHEED oscillations are maintained.

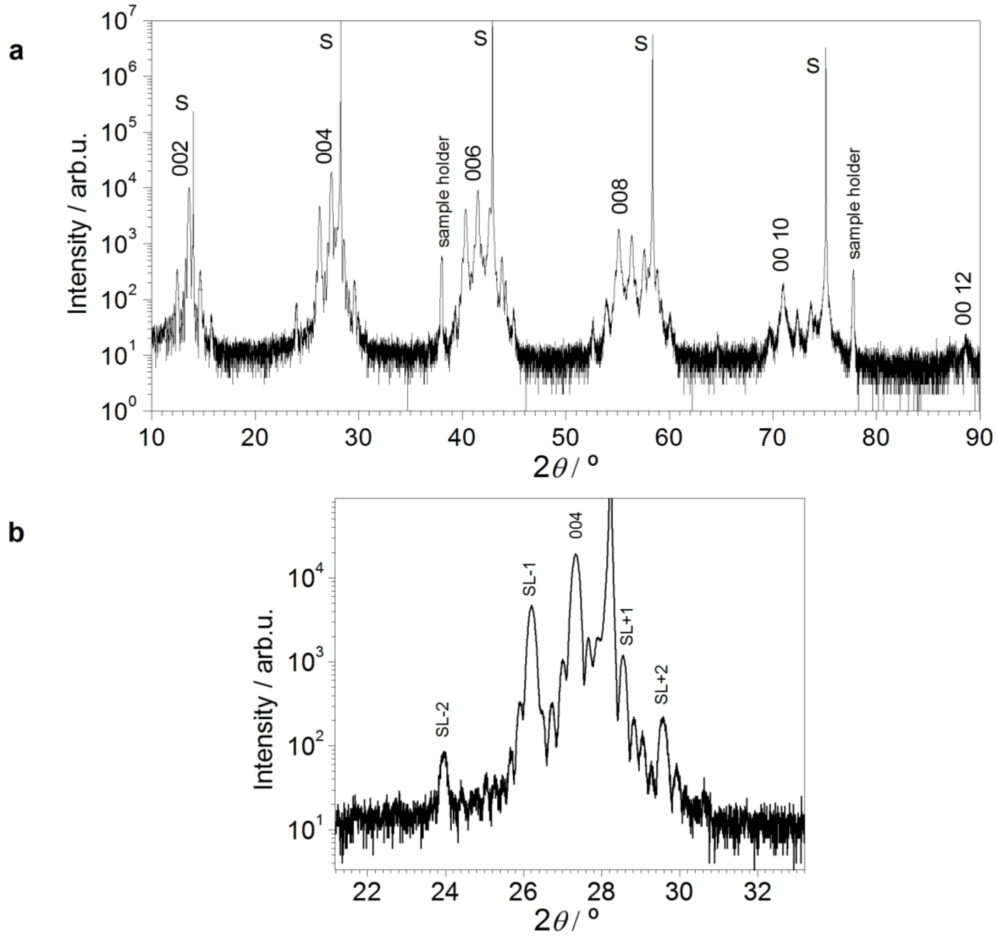

Supplementary Figure S2. a) XRD fullscan pattern of a $La_{2-x}Sr_xNiO_4/La_2CuO_4$ superlattice (S = 5, N = 3.5) on $LaSrAlO_4$ (001). Substrate reflections are indicated as S. b) Magnification of the 004 Bragg peak. Superlattice peaks can be clearly observed.

***x* = 0.8**

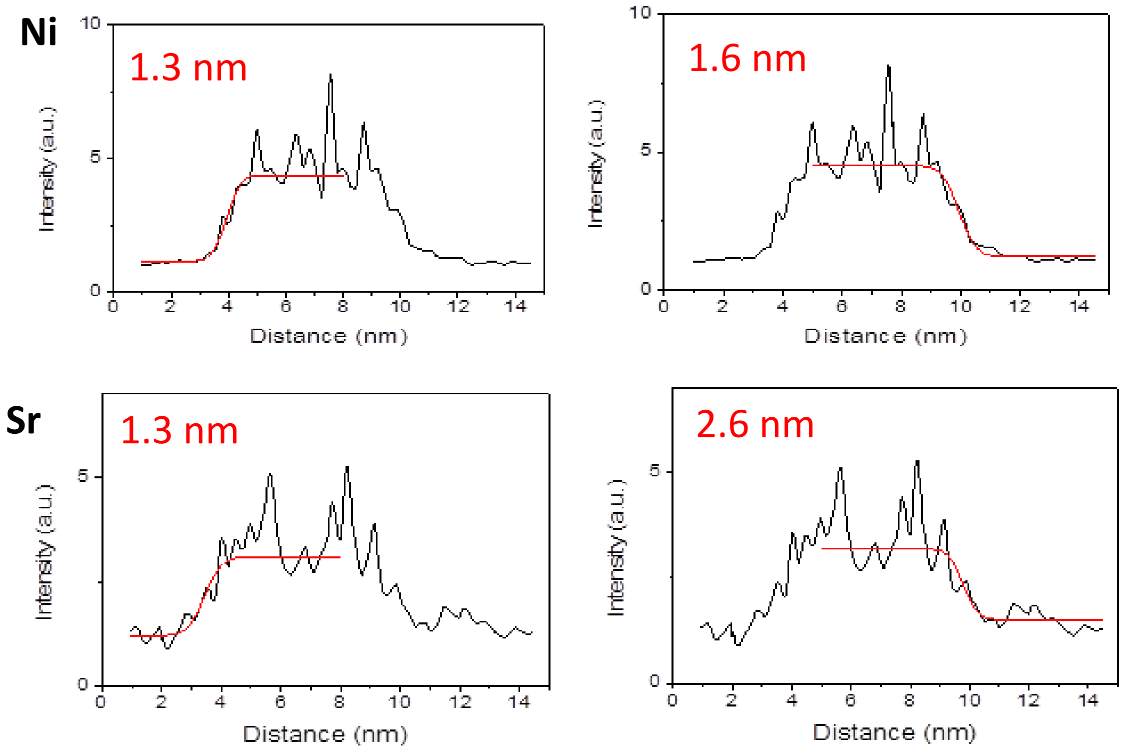

Ni
Sr
1.3 nm
1.6 nm
1.3 nm
2.6 nm
Intensity (a.u.)
Distance (nm)

***x* = 0.4**

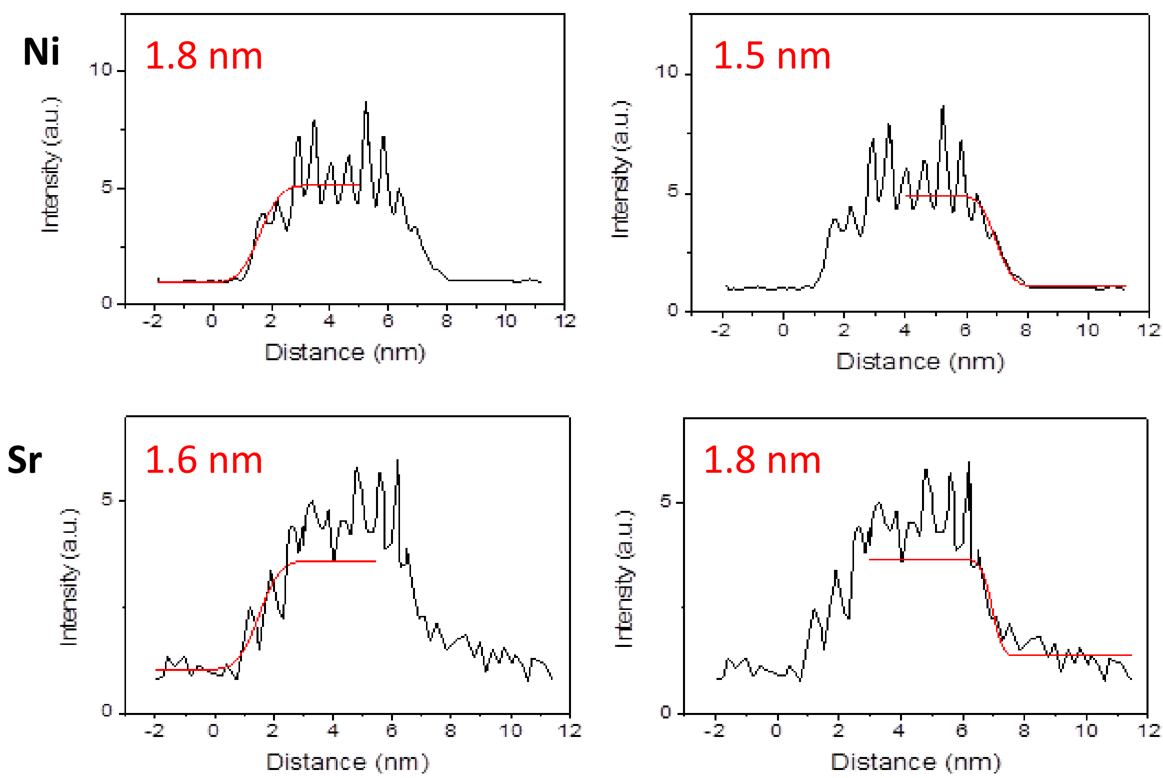

Ni
Sr
1.8 nm
1.5 nm
1.6 nm
1.8 nm
Intensity (a.u.)
Distance (nm)

	Element	x = 0.4	x = 0.8
Slope	Ni	1.8 ± 1.3 / 1.5 ± 0.9	1.3 ± 0.5/ 1.6 ± 0.9
	Sr	1.6 ± 1.1 / 1.8 ± 1.3	1.3 ± 1.1/ 2.6 ± 3.5
Tail	Ni	0 / 0	0 / 0
	Sr	0 / 2.2	0 / 3.5

Supplementary Figure S3. Broadening of elemental concentrations at lower (LCO/LSNO)/upper (LSNO/LCO) interface (in nm). The slope values are obtained by an error-function fit (which does not describe the tail) whereas the tail values correspond to the distance where the tail reaches the noise level.

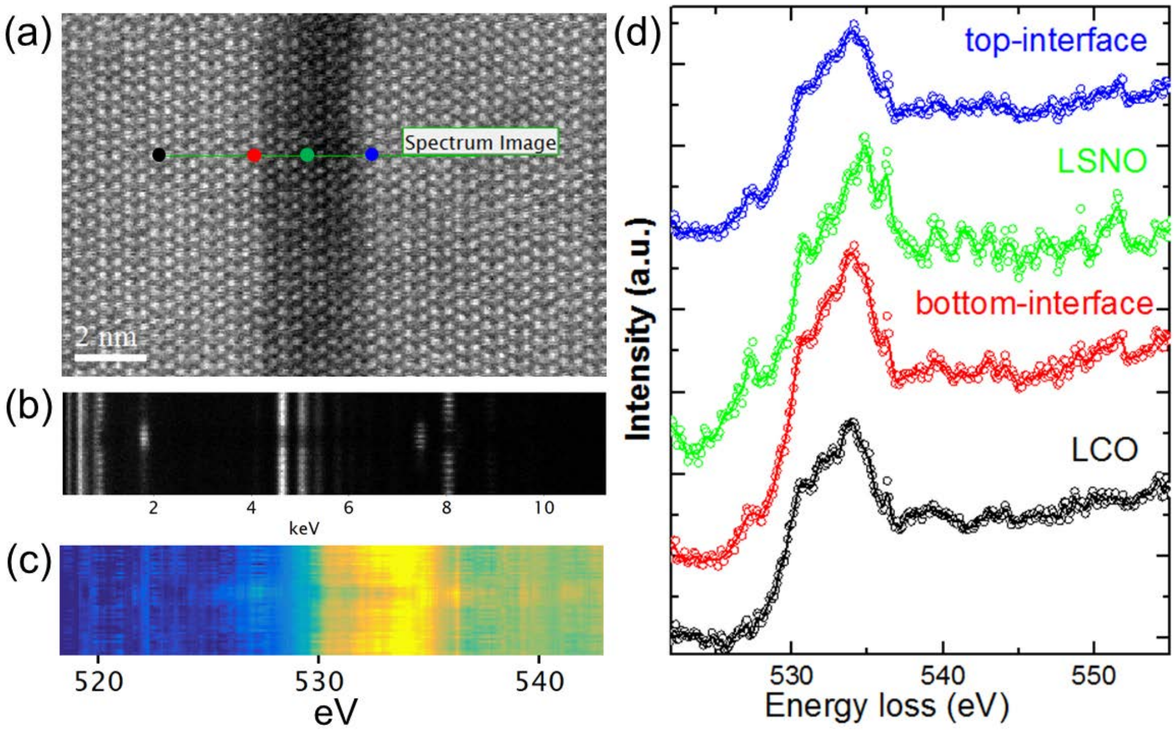

Supplementary Figure S4. (a) Survey image showing the line along which the EELS and EDXS line scan was acquired. (b) Raw EDXS spectrum image. (c) EELS spectrum image of the O-K edge after background subtraction. (d) Oxygen-K edge from different positions as indicated in Figure (a). The intensity of the pre-edge peak has been quantified by multi-Gaussian peak fitting using a non-linear least square (NLLS) routine for all spectra in the line scan profile across several interfaces.[45]

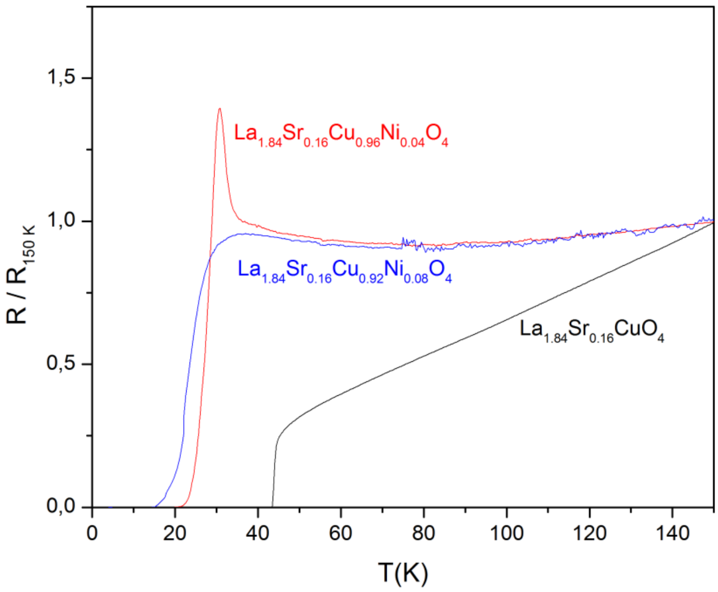

Supplementary Figure S5. Resistivity curves for optimally doped LSCO and for Ni-doped LSCO ($La_{2-x}Sr_xCu_{1-y}Ni_yO_4$).

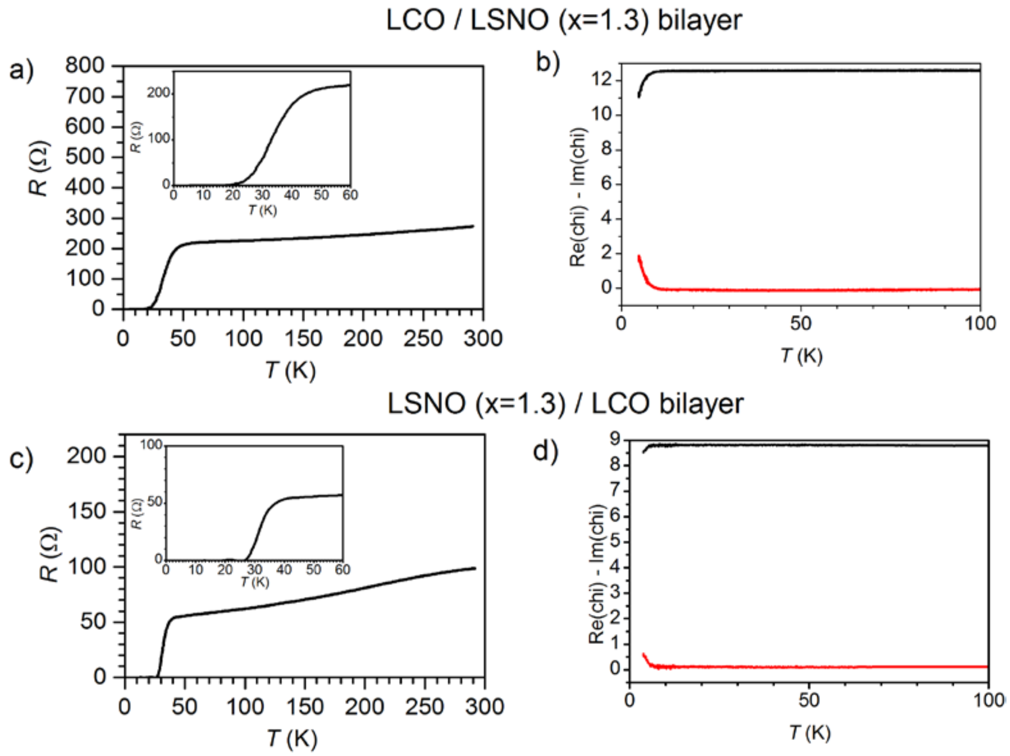

Supplementary Figure S6. Comparison between *R* vs *T* for representative LCO / LSNO - LSNO / LCO bilayers (panels a and c, respectively) and mutual inductance measurements of the diamagnetic screening (in panel (b) for LCO / LSNO and in (d) for LSNO / LCO).

Doping level x	$T_{c,}$ 0.9 (K)	T_c (K)	Transition width (K)
0,57	28,8	19	9,8
0,62	39,8	30,1	9,7
0,8	37,2	32,5	4,7
0,9	48,8	39,6	9,2
1	43,2	34,8	8,4
1,3	42,8	38,9	3,9

N	$T_{c,}$ 0.9 (K)	T_c (K)	Transition width (K)
1,5	20,3	33,4	13,1
2,5	39,1	42,3	3,2
3,5	36,7	42,9	6,2
4,5	36,5	47,3	10,8
5,5	29,2	36,6	7,4
6,5	28,1	38,8	10,7

Supplementary Table S1. Superconducting transition values for LCO/LSNO superlattices having formula 1 x $La_{1.56}Sr_{0.44}CuO_4$ + S x (2.5 x $La_{2-x}Sr_xNiO_4$ + N x La_2CuO_4), as a function of x (N = 2.5) and N (x = 2.5). The critical temperature of the superconducting transition (T_c) and $T_{c,}$ 0.9 were determined as the temperatures at which the resistance drops to the 10% and 90% of the "normal state" resistance, respectively.